Role of Anharmonicity in Dictating the Thermal Boundary Conductance across Interfaces Comprised of Two-Dimensional Materials

Sandip Thakur and Ashutosh Giri*

Department of Mechanical, Industrial, and Systems Engineering, University of Rhode Island, Kingston, Rhode Island 02881, USA

(Received 9 February 2023; revised 14 April 2023; accepted 15 June 2023; published 18 July 2023)

Understanding the fundamental heat-transport mechanisms across interfaces comprised of two-dimensional (2D) materials is crucial for the further development of the next generation of optoelectronic devices based on 2D heterostructures for which one of the main factors affecting the device performance is their poor thermal management. Here we use systematic atomistic simulations to unravel the influence of anharmonicity in dictating the thermal boundary conductance across graphene and MoS_2-based 2D and three-dimensional (3D) interfaces. Specifically, we conduct nonequilibrium molecular dynamics simulations on computational domains with graphene or MoS_2 layers encapsulated between crystalline or amorphous silicon leads across a wide temperature range (of 50–600 K). We show that while the interfacial conductance across a graphene and crystalline silicon interface demonstrates considerable temperature dependence, the conductance across a graphene and amorphous silicon interface has no significant temperature dependence. In contrast, the thermal boundary conductance for the MoS_2-based heterostructures with both the crystalline and amorphous leads demonstrate no significant temperature dependence. Our spectral energy-density calculations along with our spectrally resolved heat-flux accumulation calculations on the various interfaces show that anharmonic coupling across the entire vibrational spectrum as well as the strong hybridization of a broader spectrum of the flexural modes with substrate Rayleigh waves in graphene heterostructures give rise to the relatively higher and drastically different heat-transport mechanisms across these interfaces as compared to the MoS_2-based heterostructures. Through these understandings, we show that one strategy to enhance heat conductance across 2D-3D interfaces is to increase the anharmonic coupling between the acoustic and optic modes in the 2D materials by inducing a stronger interaction strength with the substrates. Our findings elucidate the fundamental heat-transfer mechanisms dictating thermal-boundary conductances across 2D-3D interfaces and will be crucial for heat dissipation in the next generation of optoelectronic devices where the utilization of 2D materials are becoming ubiquitous.

DOI: 10.1103/PhysRevApplied.20.014039

I. INTRODUCTION

Combining the remarkable properties of layered two-dimensional (2D) semiconductors with the advantages of bulk materials, 2D and three-dimensional (3D) heterostructures have garnered considerable interest in the past two decades both from fundamental physics as well as applicative standpoints. For instance, the integration of 2D materials such as MoS_2 and graphene in field-effect transistors (FETs) provides an avenue for excellent electrostatic gate control performances [1–3] and can potentially extend Moore's scaling law beyond the current silicon-based FETs [4]. This is possible because of the pristine interfaces associated with 2D heterostructures that form weak van der Waals interactions with the underlying layers, thus removing the constraints of lattice mismatch and the negative impact of dangling bonds that can lead to performance degradation in conventional FETs [5]. However, one of the main factors limiting the performance of nanoelectronics (such as FETs) that utilize 2D-3D heterostructures is the large thermal-boundary resistance at the weak van der Waals interfaces that poses as a major challenge for their proper thermal management [6–8]. Therefore, one of the key challenges in incorporating 2D-3D heterostructures to impact 2D optoelectronics [9], nanophotonics [10], and next-generation computing technologies [11] is the comprehensive understanding of heat-transfer mechanisms dictating thermal-boundary conductance (h_K) across 2D-3D interfaces.

A considerable amount of work in the last few years has been devoted to understanding h_K across interfaces comprised of 2D materials. Overall, both experimental and theoretical works have shown that h_K across these interfaces are in the lower end of the spectrum

*ashgiri@uri.edu

for solid-solid interfaces mainly because of the weak interaction of the 2D layer with the underlying materials [6,12]. Experimentally, Raman spectroscopy [7,13, 14], pump-probe thermoreflectance [15–17], 3ω technique [18,19], and electrical thermometries [20,21] have been utilized to report h_K in the range of approximately 10–35 MW m^{-2} K^{-1} for various 2D-3D interfaces, which is equivalent to the resistance offered by approximately 40–100-nm-thick SiO_2 layer [16,17,20,22,23].

To understand the microscopic mechanisms dictating the low thermal conductances associated with interfaces comprised of 2D materials, a considerable amount of work has also focused on atomistic simulations [24–30] as well as analytical and theoretical framework developments [8,31–36]. One of the major findings from these works is that h_K across dimensionally mismatched 2D-3D interfaces is mainly driven by the coupling between flexural modes of the 2D material and the longitudinal phonons in the underlying substrate [8,25,33]. For instance, Persson *et al.* [32,33] derived a theoretical model for h_K by accounting for the strength of interaction between the 2D material and the substrate, and (in reasonable agreement with experiments) predicted the h_K to be approximately 25 MW m^{-2} K^{-1} between a weakly coupled graphene/SiO_2 interface. Ong *et al.* [34] further modified this theoretical model by adding a superstrate (a top encapsulating layer), which led to an increase in the heat-transfer efficacy across the graphene/SiO_2 interface (with a value of $h_K = 105$ MW m^{-2} K^{-1} at room temperature that is in excellent agreement with experimental results from Chen *et al.* [18]). This increase was ascribed to additional channels of heat transfer that arise due to the coupling of the low-frequency flexural modes of the graphene with the Rayleigh phonon modes from the superstrate. Similarly, the relevance of flexural modes was further highlighted by Correa *et al.*, [31] where the authors defined a heat flux across dimensionally mismatched interfaces by incorporating a phonon-substrate interaction rate and first-principles calculated phonon dispersion relations as input parameters in their model. By comparing the results for heterostructures based on MoS_2 and graphene, they showed that a better overlap between the flexural modes and the substrate vibrational density of states (DOS) along with a stronger adhesion between the 2D material and 3D substrate resulted in a higher h_K across the graphene interface as compared to the MoS_2 interface [31]. Furthermore, utilizing the similar methodology, Foss *et al.* [8] calculated h_K across six common 2D materials and seven different substrates to highlight the role of the substrate properties such as mass density and sound speed that play a pivotal role (along with the flexural modes of the 2D material) while considering the heat-transfer efficacy across 2D-3D interfaces. Although these works have helped shed light on the microscopic dynamics dictating h_K across 2D material interfaces, a complete understanding of the spectrally resolved interfacial conductance (such as the role of anharmonic coupling in the 2D layer) for 2D-3D heterostructures is still missing.

Herein, through systematic atomistic simulations, we show that along with the relevance of flexural modes and the strength of interaction between the 2D material and the 3D substrate, the intrinsic anharmonicity and the strength of coupling between the modes of the 2D material dictates the temperature-dependent h_K across the dimensionally mismatched 2D-3D interfaces. More specifically, by considering MoS_2 and graphene on amorphous or crystalline silicon leads, we show that one of the main reasons for the higher interfacial conductances across the graphene-based interfaces is from the better coupling of the acoustic modes with the optical modes in graphene as compared to MoS_2. Furthermore, through our nonequilibrium molecular dynamics (NEMD) simulations, we show that while the h_K across a graphene and crystalline silicon interface demonstrates considerable temperature dependence, h_K across a graphene and amorphous silicon interface has no significant temperature dependence. In comparison, the interfaces associated with MoS_2 do not demonstrate a temperature dependence for either the crystalline or amorphous leads. This highlights the role of anharmonic scattering in the leads along with the anharmonicity of the 2D materials in dictating the h_K across 2D-3D interfaces. Moreover, our extensive analyses based on NEMD simulations, spectrally resolved heat-flux accumulation calculations, and spectral energy-density (SED) calculations demonstrate that the intrinsic anharmonicity of the 2D material dictates the efficacy of the flexural modes to couple with the phonon modes across the van der Waals interfaces. This intrinsic anharmonicity can be manipulated by varying the strength of interaction between the 2D material and the leads to drastically improve the heat-transfer efficacy across even MoS_2-based interfaces that are typically associated with large thermal boundary resistances ($1/h_K$).

II. METHODS

We perform MD simulations to predict and understand h_K across MoS_2 and graphene on amorphous or crystalline silicon substrates under the NEMD framework. For all our simulations, we utilize the large-scale atomic and molecular massively parallel simulator (LAMMPS) package [37]. We implement the Stillinger-Weber (SW) potential [38] to describe the interatomic interactions of the atoms in the MoS_2 layers. For the carbon atoms in the graphene layers, we utilize the adaptive intermolecular reactive empirical bond-order (AIREBO) potential [39], which has been utilized to study the thermal properties of graphene [40–42]. For the Si atoms, the Tersoff potential [43] is used since it has been used previously to study thermal conductivities of both amorphous and crystalline silicon domains [44–46]. The SW potential for MoS_2 has also been used in the prior

literature to study their thermal as well as mechanical properties [38,47,48]. To model the interactions between the 2D monolayer and the 3D substrate, we use the Lennard-Jones (LJ) potential, which is given as [49]

$$U = \sum_{i,j} 4\epsilon_{ij} \left[\left(\frac{\sigma_{ij}}{r_{ij}} \right)^{12} - \left(\frac{\sigma_{ij}}{r_{ij}} \right)^{6} \right]. \quad (1)$$

Here ϵ_{ij} and σ_{ij} are the characteristic parameters of energy and distance, respectively. The parameters for the different interactions are chosen based on the widely used universal force field [49]. Further details regarding the simulations and specific parameters for the LJ potential are given in the Supplemental Material [50].

Initially the structures are equilibrated under the Nosé-Hoover thermostat and barostat (i.e., the NPT ensemble) [51] for 2 ns with a timestep of 0.5 fs where the number of particles, pressure, and temperature of the system are held constant at 0 bar pressure. Following the NPT integration, further equilibration is carried out under the NVT ensemble where the volume and temperature are kept constant for a total of 1 ns with periodic boundary conditions for the entire simulation. An additional equilibration is performed under NVE ensemble for 1 ns where the number of particles, volume, and total energy of the system are maintained constant.

Figure 1 shows the schematic representations of parts of our equilibrated computational domains for our MoS_2 and graphene monolayers supported on crystalline silicon (c-Si) and amorphous silicon (a-Si) substrates. Even though we show only part of our computational domains (clearly showing the 2D-3D interfaces) in Fig. 1, we note that our NEMD simulations are carried out on sandwiched 2D structures that are encased between two semi-infinite leads. The leads are considered as semi-infinite because their prescribed lengths do not affect our predictions of h_K across the different 2D-3D interfaces. To make the amorphous Si substrates, we use the melt-quench technique [52–54] where a crystalline Si domain is initially melted at 4000 K, followed by rapid quenching to form an amorphous Si substrate. The structure is then allowed to equilibrate under the Nosé-Hoover thermostat and barostat [51], which is the NPT ensemble (with the number of atoms, pressure, and temperature held constant) for a total of 1 ns at a prescribed temperature and ambient pressure conditions.

To determine h_K across our 2D-3D interfaces, we implement the NEMD method where we impose a heat flux, q, across the equilibrated computational domain in order to establish a steady-state spatial temperature gradient as shown in Fig. 2 for our characteristic a-Si/MoS_2 heterostructure. This is carried out by prescribing a "hot" region located at one end of the computational domain where we add energy at a constant rate and extracting the equal amount of energy from the "cold" region located at

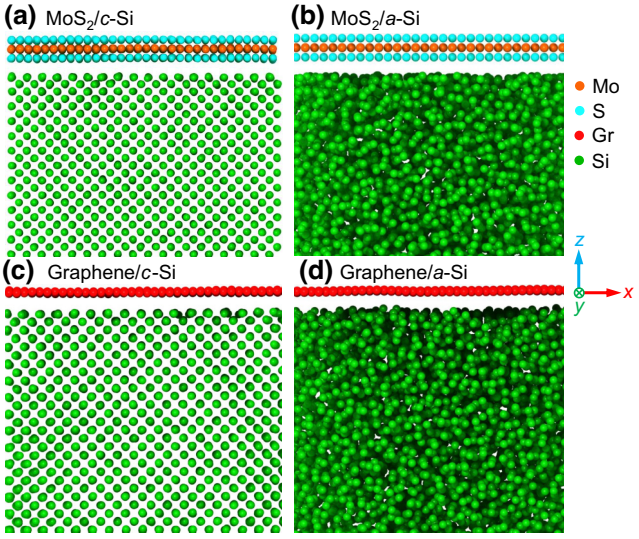

FIG. 1. Schematic illustrations of parts of our computational domains for (a) MoS_2/c-Si, (b) MoS_2/a-Si, (c) graphene/c-Si, and (d) graphene/a-Si structures used for our atomistic simulations. Note, the schematics are only showing part of the domains to highlight the different interfaces studied in this work. We perform our calculations on structures with the 2D material encased between two semi-infinite silicon leads.

the other end of the computational domain. We partition our computational domain into different regions along the z direction as shown in Fig. 2(a), where the atoms in the "wall" region are held fixed, while a fixed amount of heat is added and removed from the atoms in the "hot bath" and "cold bath" regions, respectively. Note, the "wall" and the "bath" regions are each approximately 20 Å thick. In order to create a steady-state temperature profile across the z direction of our computational domains, we apply a heat flux ($q = 0.8$ GW m^{-2}) by adding a constant amount of kinetic energy (2.3×10^{-5} J s^{-1}) to the "hot" region and removing the equal amount of energy from the "cold" region. For the temperature profiles, we divide the atoms in the computational domain into 100 equally sized bins along the direction of the applied heat flux. The temperature of the atoms in each bin is averaged after achieving steady state, which results in a temperature profile as shown in Fig. 2(b) for the case of our MoS_2/a-Si domain. Finally, after we obtain a steady-state temperature profile, the h_K is calculated through the relationship given as

$$h_K = \frac{q}{\Delta T}. \quad (2)$$

Here ΔT is the temperature difference across the 2D-3D interface, which is determined from the temperature profiles.

To ensure our results are not influenced by the size of our computational domains, we carry out a series of

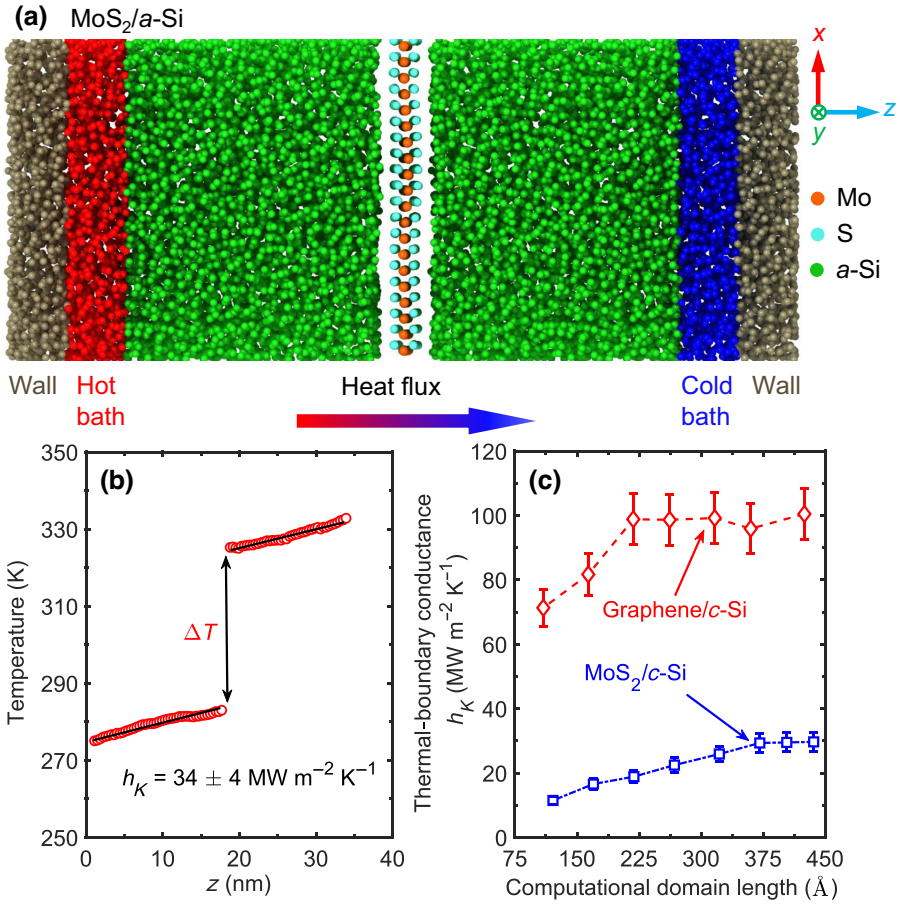

FIG. 2. (a) Schematic illustration of the computational domain for our MoS_2/a-Si structure used in our NEMD simulations to predict the thermal-boundary conductance across MoS_2/a-Si interface. (b) Steady-state temperature profile obtained from our NEMD simulation, which we utilize to calculate the thermal-boundary conductance across MoS_2/a-Si interface. (c) NEMD simulation-predicted h_K as a function of computational domain length (by varying the lengths of the silicon leads) for MoS_2/c-Si and graphene/c-Si heterostructures. The h_K values converge for domain sizes greater than approximately 225 Å and approximately 375 Å for our graphene/c-Si and MoS_2/c-Si structures, respectively.

NEMD simulations by varying the length of the silicon leads in our simulation domain with total domain lengths of approximately 110 Å to approximately 436 Å along the direction of the applied heat flux as shown in Fig. 2(c). The convergence of thermal-boundary conductance within uncertainties for computational domain sizes greater than approximately 225 Å and approximately 375 Å for our graphene/c-Si and MoS_2/c-Si structures, respectively, ensures that our choice of the domain sizes do not influence our NEMD-predicted h_K values for both the MoS_2- and graphene-based heterostructures. The uncertainties in our reported h_K values are determined from five independent simulations along with the 95% confidence intervals based on fitting the temperature profiles of the silicon leads to obtain the temperature drops at the 3D-2D-3D interfaces.

We calculate the phonon-mode-specific properties of our unconstrained and encapsulated 2D structures in between the semi-infinite leads by utilizing the SED approach. In this technique, the atomic motion trajectories are Fourier transformed to get the average kinetic energy per unit cell at a specific wave vector (**k**) and frequency (ω), which is calculated as [55,56],

$$\Phi(\mathbf{k},\omega) = \frac{1}{4\pi\,\tau_0 N_T}\sum_{\alpha}^{3}\sum_{j}^{B} m_j \left| \int_0^{\tau_0} \sum_{n_{x,y,z}}^{N_T} \dot{u}_\alpha \begin{pmatrix} n_{x,y,z} \\ j \end{pmatrix}; t \right) \times \exp\left[i\mathbf{k}\cdot\mathbf{r}\begin{pmatrix} n_{x,y,z} \\ 0 \end{pmatrix} - i\omega t \right] dt \Bigg|^2 . \quad (3)$$

Here τ_0 is the total simulation time, N_T is the number of unit cells in the crystal, α is the Cartesian direction, B is the atomic number in the unit cell, j is the atom label in a given unit cell, m_j is the mass of jth atom in the unit cell, $n_{x,y,z}$ is a unit cell, $\dot{u}_\alpha$ denotes the velocity along the α

direction at time t and $\mathbf{r}$ is the equilibrium position of each unit cell.

To ensure a high resolution in our SED calculations, we construct a larger simulation domain (approximately 45×6 nm^2 in the x and y directions) and extract 75 $\mathbf{k}$ points along the Γ to M direction. We equilibrate our supercell structure initially under the Nosé-Hoover thermostat and barostat [51] for 2 ns with a timestep of 0.5 fs where the number of particles, pressure, and temperature of the system are held constant at 0 bar pressure. Following the NPT integration, further equilibration is carried out under the NVT ensemble for another 2 ns. Finally, for the data collection for our SED calculations, we output the velocities and positions of each atom using the microcanonical ensemble (or NVE ensemble) for 1.5 ns.

To quantify the contributions of the specific vibrational frequencies to the total heat flow across the 2D-3D interfaces, we calculate the spectral heat-flux accumulation that is given as [57,58]

$$Q = \int_0^\infty \frac{d\omega}{2\pi} q(\omega). \tag{4}$$

Here ω is the angular frequency and $q(\omega)$ is the spectral heat current. This heat current is proportional to the correlation between the interatomic force between the atoms across the interface and the velocities,

$$q_{i\to j}(\omega) \propto \langle \overrightarrow{F}_{i,j} \cdot (\overrightarrow{v}_i + \overrightarrow{v}_j) \rangle. \tag{5}$$

Here the spectral heat current between atoms i and j is proportional to the correlation between the force of two atoms, $\overrightarrow{F}_{i,j}$ and their velocities, $\overrightarrow{v}_i$ and $\overrightarrow{v}_j$. For spectral heat-flux accumulation calculations, we collect the atomic forces and velocities for a total of 1 ns at a sampling interval of 5 fs. Further details of the spectral heat-flux calculations are given in our prior work in Ref. [58].

III. RESULTS AND DISCUSSION

Figure 3 shows our calculated temperature-dependent h_K values for our 2D-3D interfaces across the temperature range of 50–600 K. Our predicted h_K values of approximately 29 MW m^{-2} K^{-1} and approximately 34 MW m^{-2} K^{-1} for monolayer MoS_2 sandwiched between crystalline and amorphous leads, respectively, agree well with prior results [13,59]. For instance, Gabourie *et al.* [59] report a value of $h_K = 34.3$ MW m^{-2} K^{-1} for MoS_2 on Al_2O_3 substrate at room temperature with an approach to equilibrium MD method. Yalon *et al.* [13] experimentally measured a value of $h_K = 14 \pm 4$ MW m^{-2} K^{-1} at room temperature for MoS_2 encased between an AlO_x layer and a SiO_2/Si substrate using Raman thermometry. Similarly, for our graphene/c-Si interface, we predict $h_K = 98$ MW m^{-2} K^{-1}, which is in good agreement with the experimentally determined value of 83 MW m^{-2} K^{-1} for the graphene/SiO_2 interface [18]. The slight discrepancies between the prior results and our MD results might arise due to the varying substrates, which (as we discuss below) can have a major influence on the interfacial conductance across 2D-3D interfaces.

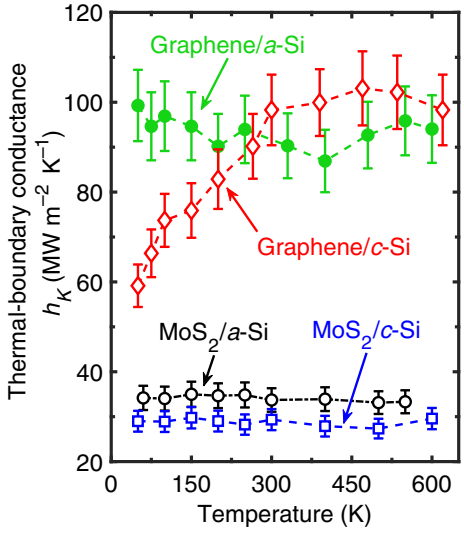

FIG. 3. Nonequilibrium molecular dynamics simulation-predicted thermal-boundary conductances (h_K) as a function of temperature for MoS_2/c-Si, MoS_2/a-Si, graphene/c-Si, and graphene/a-Si heterostructures. The h_K across the 2D-3D interfaces are derived from structures where the 2D material is encapsulated between two semi-infinite leads. The increasing trend in h_K with temperature for the graphene/c-Si interface suggests that anharmonic scattering largely dictates the h_K across this interface.

As shown in Fig. 3, the h_K values predicted for both the MoS_2/c-Si and MoS_2/a-Si interfaces show no temperature dependencies across the entire temperature range. In contrast, the graphene-based interfaces demonstrate drastically different thermal characteristics where the h_K across the graphene/c-Si interface shows considerable temperature dependence, whereas the h_K across the graphene/a-Si interface is temperature independent. These drastically different temperature trends for the MoS_2- and graphene-based interfaces show that the fundamental heat-transfer mechanisms dictating h_K across these interfaces are characteristically different. For instance, the increasing h_K across the graphene/c-Si suggests that anharmonic interactions are more prevalent for this interface as compared to the others. Furthermore, the fact that replacing the crystalline leads with amorphous systems results in the lack of temperature dependence of h_K indicates that anharmonic interactions in the leads (and not just limited to the 2D layer) also dictates the h_K across the graphene-based interfaces. In the amorphous leads, disorder scattering dominates over anharmonic scattering, which ultimately influences the temperature dependence (or the lack thereof)

for the h_K across graphene/a-Si interface. However, it is surprising that even for the MoS_2/c-Si interface we observe a similar temperature dependence as the MoS_2/a-Si interface. Again, the lack of temperature dependence for the MoS_2-based heterostructures indicates the lack of anharmonic scattering in dictating the interfacial conductance for these systems.

Figure 4 shows the calculated thermal boundary conductance as a function of the number of layers for our MoS_2/c-Si and graphene/c-Si structures. For both the MoS_2/c-Si and graphene/c-Si heterostructures, the h_K values do not significantly change with the increase in the number of 2D layers. The similarity in the h_K values shows that the number of 2D layers has negligible influence in dictating the thermal-boundary conductance across our 2D-3D interfaces.

As MD simulations are strictly classical in nature, all of the vibrational modes in the entire vibrational spectrum are activated at all temperatures. Thus, an increasing trend in h_K with temperature is indicative of the prevalence of anharmonic effects [57,58,60,61]. Therefore, although we cannot separate the contributions from harmonic and anharmonic processes in our NEMD simulations, the drastically different (and increasing) temperature dependence of graphene/c-Si interface signifies that inelastic processes are more prominent for this interface. However, we note that comparison to results from atomistic Green's function (AGF) calculations could lend more insights into the competing effects between elastic and inelastic processes

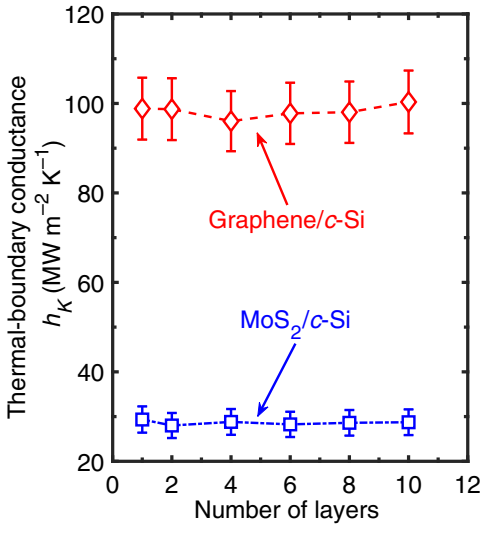

FIG. 4. Calculated h_K as a function of the number of MoS_2 and graphene layers in our MoS_2/c-Si and graphene/c-Si heterostructures, respectively. For both the MoS_2/c-Si and graphene/c-Si heterostructures, we observe negligible influence on the thermal-boundary conductance with the increase in the number of 2D layers.

[62,63], which is beyond the scope of the current work but deserves further attention.

The h_K values predicted for the amorphous leads in the MoS_2-based structures are consistently higher for the entire temperature range when compared to the crystalline leads. Moreover, h_K values predicted for graphene/a-Si interface are higher as compared to the h_K for graphene/c-Si structure at lower temperatures below 300 K. These results are consistent with prior works where h_K is reported to be higher for amorphous substrates as compared to the perfectly crystalline substrates [64,65]. This has been attributed to better vibrational coupling of the heat carrying phonons across the disordered interfaces. Furthermore, in contrast to the MoS_2-based systems, the h_K values across the crystalline and amorphous leads for our graphene-based heterostructures are similar within uncertainties at higher temperatures (> 300 K). The slightly lower h_K for the graphene/a-Si structure might be a result of competing effects between anharmonic scattering and disorder scattering across the graphene/silicon interfaces. However, within uncertainties of our NEMD simulations, a clear difference between the values predicted for h_K across graphene/c-Si and graphene/a-Si is not observed. Therefore, we cannot draw any meaningful conclusions as to the effect of disorder in the atomic arrangement of the substrates on h_K across graphene/Si interfaces at higher temperatures. In this regard, a comparison to AGF calculations that consider only harmonic effects might be useful to separate the competing effects between disorder and anharmonic scattering. Although such calculations are beyond the scope of the current work, disentangling the effects of disorder scattering and anharmonic scattering across these interfaces clearly deserves further attention. We now attempt to better explain and gain more insights into these different h_K trends through spectrally resolved heat-flux accumulation and SED calculations, as we discuss in detail below.

Firstly, to understand the intrinsic mechanisms dictating the temperature-dependent h_K values in these 2D-3D interfaces, we compare the vibrational density of states (DOS) and the spectrally resolved heat-flux accumulation calculations of the various systems in Fig. 5. As shown in Fig. 5(a), we observe significant enhancement of DOS for vibrational frequencies in the 2–4 THz range for the monolayers of silicon atoms adjacent to the 2D materials as compared to the DOS of the bulk silicon atoms. As shown by our spectrally decomposed heat-flux accumulation calculations in Fig. 5(b) for the heat flux from the silicon leads to the MoS_2 and graphene layers, the vibrational modes in this frequency range are largely responsible for coupling with the flexural modes of the 2D material to facilitate heat transport across the 2D-3D interface. It is also interesting to note that for the spectral heat flux across the silicon/graphene interface, the vibrational spectrum spans a much wider range as compared to the heat flux across the silicon/MoS_2 interface. This might not be surprising

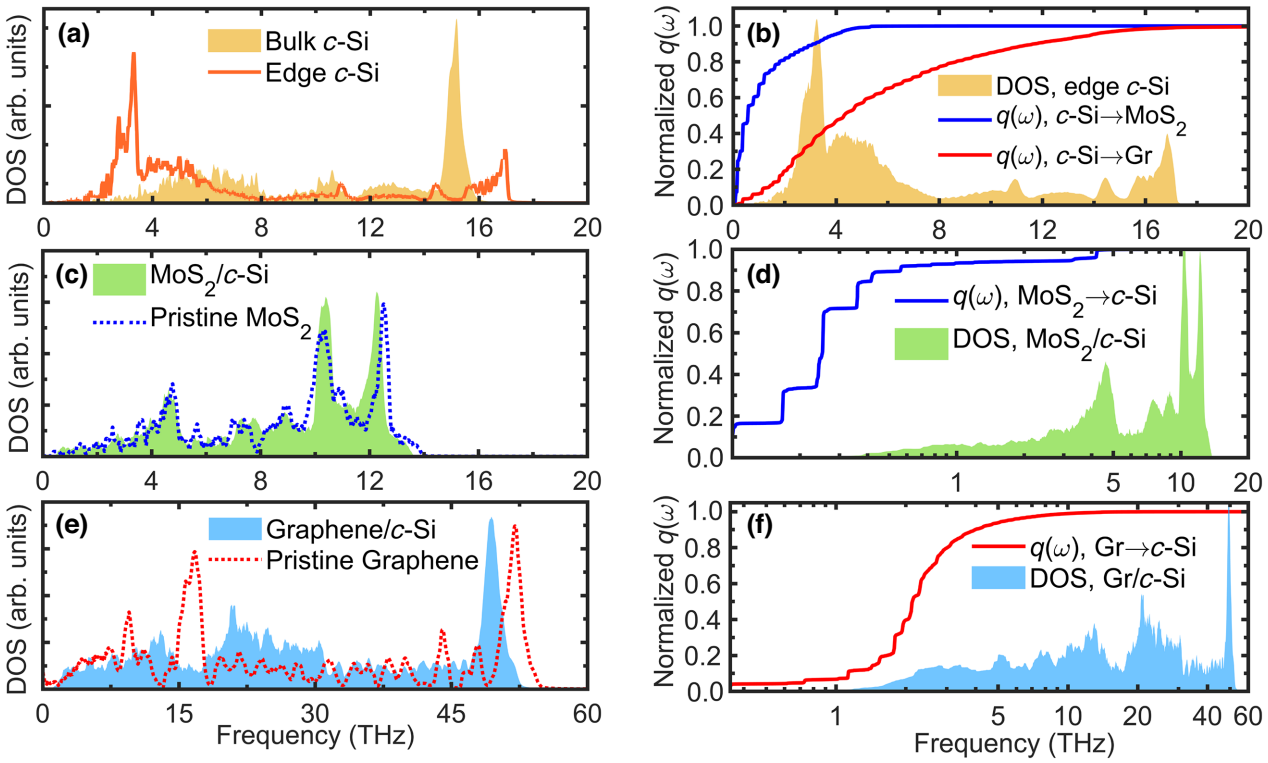

FIG. 5. (a) Vibrational DOS and (b) spectrally resolved heat-flux accumulation for monolayers of silicon atoms adjacent to the 2D materials. As compared to the DOS of the bulk silicon, frequencies in the 2–4 THz range have enhanced DOS for the interfacial monolayer of silicon atoms (edge *c*-Si). These modes are largely responsible for heat conduction across the interfaces to the adjacent 2D materials. The frequency range for transmission to the graphene layer is much broader in comparison to the MoS_2, which explains the higher h_K values for the graphene/silicon interfaces. (c) Vibrational DOS and (d) spectrally resolved heat-flux accumulation for MoS_2. The spectral region of flexural modes in MoS_2 that are responsible in carrying the heat across to the silicon leads is very narrow, which explains the higher thermal resistances associated with these interfaces. (e) Vibrational DOS and (f) spectrally resolved heat-flux accumulation for graphene. Flexural modes as high as approximately 10 THz can carry the heat across to the silicon leads, thus explaining their relatively higher values of h_K as compared to the MoS_2-based interfaces.

since the flexural ZA mode in graphene can span up to approximately 15 THz [66]. This wider frequency spectrum responsible for heat conduction across the graphene-based interfaces also helps explain its stronger anharmonic nature as compared to the MoS_2-based interfaces. Moreover, when comparing the vibrational spectrum of the MoS_2 and graphene [Figs. 5(c)–5(f)], it is evident that the stronger sp^2-bonded carbon atoms in the graphene layers results in a wider vibrational frequency spectrum. These higher-frequency acoustic and optical modes in graphene might be responsible for dictating the anharmonic nature of the interfacial heat conduction. However, as shown by our heat-flux accumulation calculations in Figs. 5(d) and 5(f) for MoS_2/*c*-Si and graphene/*c*-Si, respectively, the inefficient heat conduction across the 2D-3D interfaces, in general, can be attributed to the narrow frequency range capable of actually carrying the heat across these interfaces. Therefore, as shown by our calculations, and in agreement with prior results [8,25,33,67], the interfacial heat conduction across 2D-3D interfaces are categorically different as compared to 3D and 3D interfaces since it is only through flexural modes that heat can couple across the 2D-3D interfaces. This is in contrast to the interfacial heat transport facilitated by impinging phonons undergoing a transmission or reflection at 3D and 3D interfaces. As such, neither the DOS calculations nor the spectral heat-flux calculations can provide a complete and clear picture of the intrinsic physical processes that result in the drastically different temperature dependencies of MoS_2- and graphene-based interfaces.

To gain further insights into the intrinsic mechanisms dictating the heat transfer across our 2D-3D interfaces, we perform SED calculations [55,56]. Figures 6(a)–6(d) show the comparison of SEDs for the 2D materials with or without the leads (i.e., either encased or free standing). This comparison will help elucidate the effect of encapsulation on the vibrational heat-transport mechanisms across the interfaces. Note, the higher contrasts in the shading of the plots are related to the higher magnitudes of the SEDs. Thus, the modes that appear brighter have higher

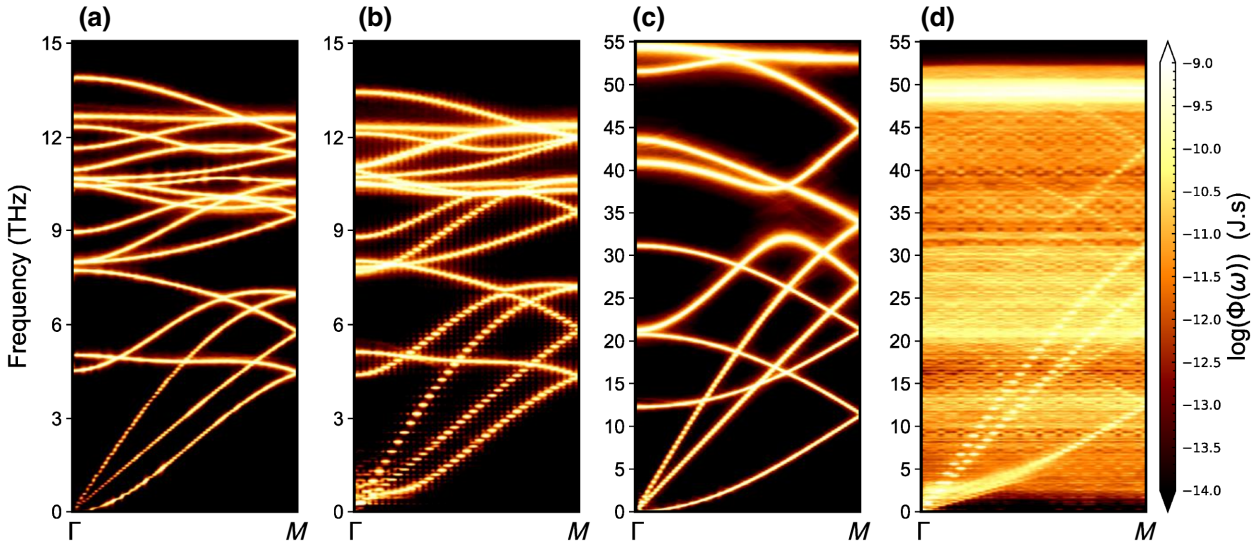

FIG. 6. Calculated phonon spectral energy densities for (a) free-standing MoS_2 monolayer, (b) MoS_2/c-Si encased structure, (c) free-standing graphene monolayer, and (d) graphene/c-Si encased structure at room temperature. The relative effect on the anharmonicity of encapsulation for graphene in between the leads is much stronger where considerable broadening of the phonon branches is observed. This signifies enhanced vibrational coupling between the acoustic and optic modes in graphene-based heterostructures as compared to the MoS_2/c-Si encapsulated structure where we do not observe a significant increase in the broadening or change in the SEDs as compared to its free-standing counterpart.

kinetic energies. Also, the broadening of SEDs suggest larger anharmonicities, stronger scattering, and reduced lifetimes of the phonon modes. For MoS_2 [Figs. 6(a) and 6(b)], the effect of encapsulation between the silicon leads on the SEDs is insignificant with minimal broadening of the vibrational modes. In contrast, for graphene [Figs. 6(c) and 6(d)], the effect of encapsulation between the leads is very evident where we observe significant broadening throughout the entire vibrational spectrum as compared to the SED of the free-standing structure suggesting considerable anharmonicities and vibrational coupling between the acoustic and optic modes when graphene is encased between the leads. This increase in anharmonicity and coupling of acoustic and optic modes results in the temperature dependence and significantly higher h_K values for graphene/c-Si structure as compared to the MoS_2 structure. Moreover, as shown in Fig. 6(d), the flexural (ZA) mode of graphene linearizes in the encapsulated case as compared to the unconstrained monolayer resulting in increased group velocities of the ZA modes. This enhancement in the group velocities and linearization of the ZA modes has been ascribed to the hybridization and coupling of graphene ZA modes to the substrate Rayleigh waves [24,68]. In fact, it has been shown that the hybridization between the substrate Rayleigh waves with the ZA modes in graphene leads to the reduction of the in-plane thermal conductivity [68]. However, when the strength of interaction between the substrate and graphene is increased, the thermal conductivity has been shown to increase due to enhanced coupling of the modes. We draw similar conclusions on the effect of the strength of interaction on h_K as we discuss later.

The hybridization between the substrate Rayleigh waves and the flexural modes is considerably less prominent for the MoS_2 structure [Fig. 6(b)], which indicates that there are significantly less channels of heat conduction from the 2D layer to the leads. This is exemplified by the much weaker broadening of the very low-frequency modes close to the Brillouin-zone center in the encased MoS_2 [Fig. 6(b)] as compared to that in the encased graphene [Fig. 6(d)]. Therefore, the h_K across MoS_2 interfaces are significantly lower than that of the anharmonic graphene interfaces (Fig. 3). Taken together, our SED calculations show that anharmonic coupling in the 2D material encapsulated between the leads can lead to higher transmission of vibrational energies through the hybridized ZA modes. As such, a viable route to increase the h_K across 2D-3D interfaces could be to increase the vibrational coupling within the 2D material itself.

To further increase the coupling of vibrational modes in the 2D material, we compress our computational domains along the direction normal to the 2D layers. Doing so, results in higher van der Waals interaction strengths between the 2D material and the leads, which has been linked to higher values of h_K across 2D-3D interfaces in prior works [20,67]. Note, to determine the interlayer interaction strengths across our 2D-3D interfaces, we calculate the total pairwise interaction forces between the two groups of atoms (the first group consisting of the MoS_2 or the graphene monolayer and the second group consisting

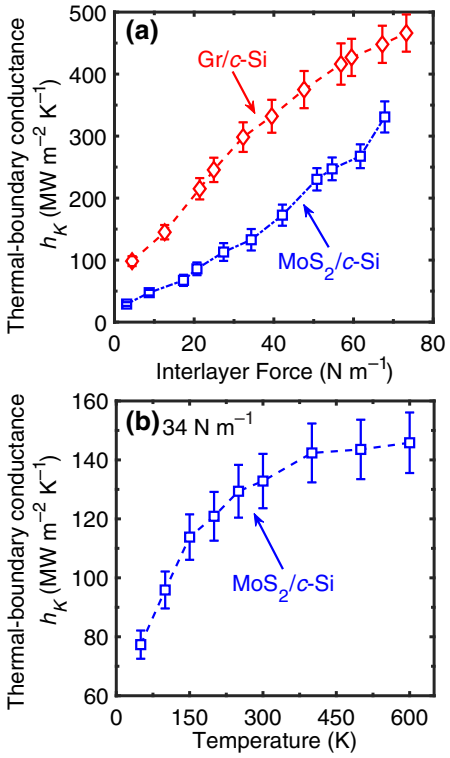

FIG. 7. (a) Calculated thermal-boundary conductances, h_K as a function of interlayer interaction strengths for MoS_2/c-Si and graphene/c-Si heterostructures. For both MoS_2/c-Si and graphene/c-Si interfaces, h_K increases monotonically with increasing van der Waals interaction strength. (b) NEMD-predicted h_K for MoS_2/c-Si structure showing an increased temperature dependence when the interlayer interaction strength is increased to 34 N m^{-1}. This suggests that increasing the van der Waals interaction strength between MoS_2 and silicon results in greater anharmonic interactions and therefore a greater temperature dependence of h_K across the MoS_2/c-Si interface.

of a monolayer of silicon atoms adjacent to the 2D layer). The forces are averaged over a period of 0.5 ns in our simulations and the interaction strengths are normalized by the characteristic distance between the 2D layers and the 3D substrates. As shown in Fig. 7(a), we also observe a monotonically increasing h_K across both the graphene and MoS_2 interfaces with increasing interaction strengths between the dimensionally mismatched interfaces. However, as expected, the graphene-based structures possess higher h_K values for the entire range of interaction strengths as compared to the MoS_2-based structures. More interestingly, we find that for MoS_2/c-Si computational domains with stronger interaction strengths, the NEMD-predicted h_K shows an increased temperature-dependence where h_K increases with increasing temperature as shown in Fig. 7(b) for the domain with the interaction strength of 34 N m^{-1}. This is in contrast to the lack of temperature dependence of the h_K for the uncompressed MoS_2/c-Si interface as shown in Fig. 3. This suggests that the h_K for the MoS_2/c-Si domains with higher van der Waals interaction strengths could largely be driven by enhanced anharmonic vibrational scattering mechanisms in the MoS_2 layer. These anharmonic processes could be a major factor in increasing the interfacial conductances for the highly thermally resistive MoS_2-based interfaces.

To support this hypothesis and to dig deeper into the intrinsic mechanism behind the temperature-dependent h_K in these materials, we further calculate the SEDs with increasing interlayer interaction strengths between the 2D-3D interfaces as shown in Fig. 8. For the MoS_2/c-Si structure [Figs. 8(a)–8(c)], anharmonicity increases with increasing interlayer interaction strengths as evident from the increased broadening of the linewidths of the high-frequency optical and acoustic branches. This suggests stronger coupling of the acoustic and optical modes in the MoS_2 layer leading to the higher values of h_K with increasing interaction strengths as shown in Fig. 7(a). Furthermore, the quadratic flexural mode also tends to linearize with increasing interaction strengths. In line with our SED calculations, our spectrally resolved heat-flux calculations show that the increasing van der Waals strength leads to an increase in the spectrum of flexural modes that are capable of carrying the heat across the 2D-3D interfaces [Fig. 8(d)]. This is shown by the shift to higher frequencies of the contributions to the spectral heat flux across the MoS_2/c-Si interface with increasing interaction strengths. For the graphene-based systems [Figs. 8(e)–8(g)], the increased effect of anharmonicity arising from the stronger interaction between the graphene and the leads is not so evident since the SEDs of the modes in the graphene-based domains already show pronounced anharmonicity even for the uncompressed structure. However, we do observe increasing group velocities of the hybridized ZA modes with increasing interaction strengths. Complementary spectrally decomposed heat-flux accumulation also show a broader range of frequencies that are capable of transporting heat across the graphene/silicon interfaces [Fig. 8(h)]. This increase in the frequency spectrum as well as the increased group velocities of the flexural modes explains the monotonically increasing h_K of the graphene/c-Si interface as shown in Fig. 7(a).

Our study reveals the fundamental mechanisms affecting the thermal-boundary conductance across 2D-material interfaces by utilizing systematic atomistic simulations. Our results have major implications on the interpretation of experimental results measuring h_K across 2D-3D heterostructures that are ubiquitous in our current technology. For instance, 2D MoS_2 monolayers have been considered as alternative channel materials for atomically thin transistors [1], flexible electronics [69], and optoelectronics [70]. However, experimental measurements have demonstrated ultralow values of h_K across MoS_2 interfaces, which exposes the major thermal management issue originating at the 2D-3D interfaces in

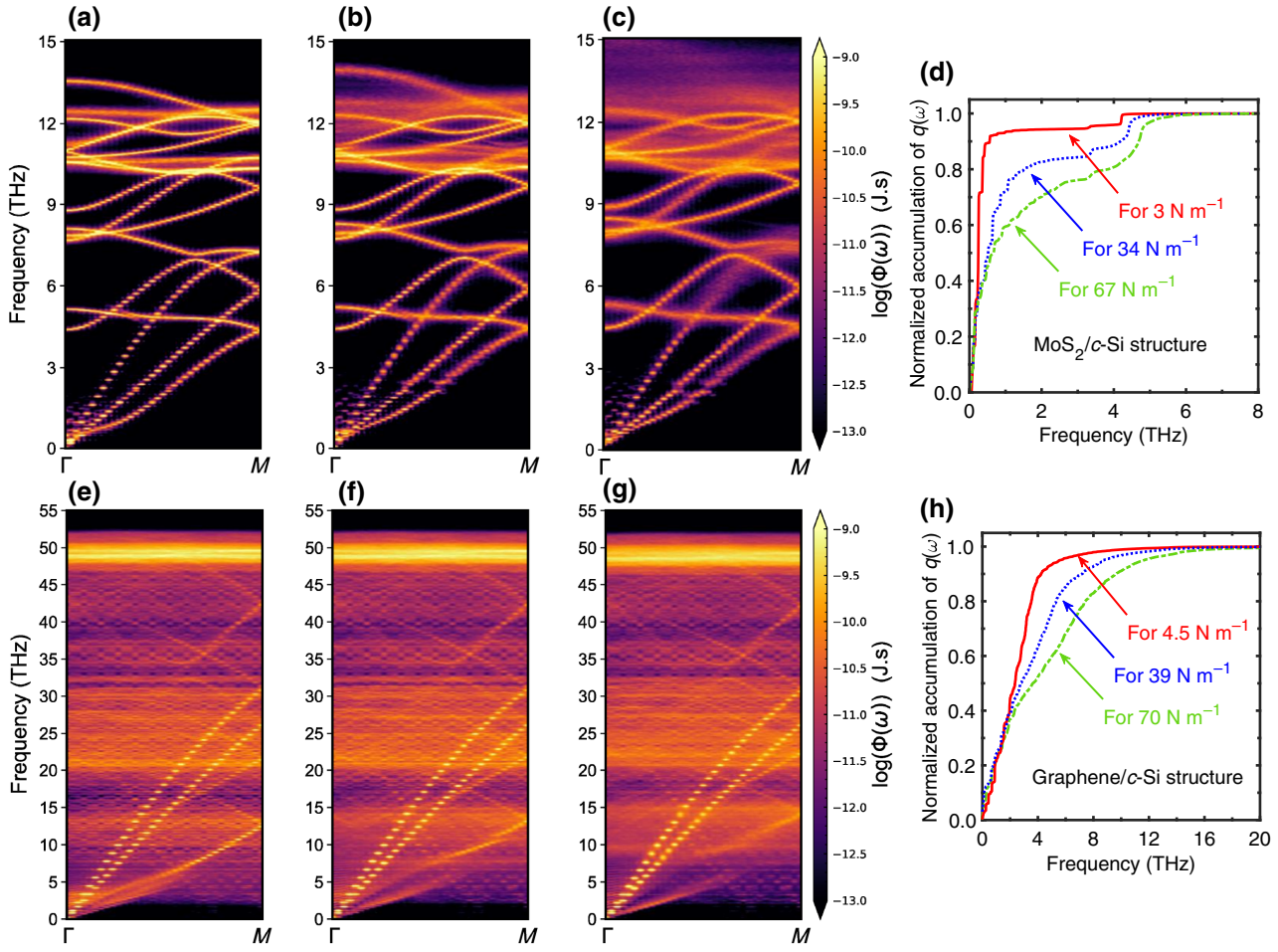

FIG. 8. Calculated phonon spectral energy densities at room temperature for MoS_2/c-Si structure with (a) 5 N m^{-1}, (b) 34 N m^{-1}, and (c) 67 N m^{-1} van der Waals interaction strengths. (d) Spectrally resolved heat-flux accumulation for MoS_2 with varying interlayer interaction strengths. With increasing interaction strengths, the contribution to the interfacial conductance shifts to higher flexural frequencies. Calculated phonon spectral energy densities at room temperature for graphene/c-Si structure with (e) 6 N m^{-1}, (f) 39 N m^{-1}, and (g) 70 N m^{-1} van der Waals interaction strengths. (h) Spectrally resolved heat-flux accumulation for graphene with varying interlayer interaction strengths. Similar to the MoS_2 case, with increasing interaction strengths, the contribution to the interfacial conductance shifts to higher flexural frequencies. In line with the spectral heat-flux calculations, for the MoS_2/c-Si structure, we observe considerably increased anharmonicities with increase in the interlayer interaction strengths as evident from the broadening of the high frequencies' optical and acoustic linewidths. Whereas, for the graphene system, although the increased anharmonicity is not so evident, the increased group velocities of the hybridized ZA modes lead to the monotonically increasing h_K with increasing interaction strengths as shown in Fig. 7(a).

these devices. Our results presented in this work show that increasing the anharmonicity across these interfaces can drastically improve h_K, thus facilitating their proper thermal management and further advancements in the above-mentioned applications. Therefore, our results can help guide the proper thermal management in devices that incorporate 2D materials by increasing interfacial heat flow through strategically engineering the 2D-3D interfaces.

IV. CONCLUSIONS

In summary, we perform systematic atomistic simulations on MoS_2- and graphene-based 2D-3D heterostructures to unravel the prominent role of anharmonic interactions in dictating their thermal-boundary conductances. More specifically, by conducting NEMD simulations on MoS_2 or graphene that is encased between two semi-infinite leads of crystalline or amorphous silicon, we find that the graphene-based heterostructures demonstrate drastically higher anharmonic interactions that are significantly weaker in the MoS_2-based structures. Our SED calculations along with our spectrally decomposed heat-flux accumulation calculations lend critical insights into the mode- and spectral-level details that dictate h_K across these 2D-3D interfaces. Through these analyses, we show that the stronger anharmonicity as well as a broader spectrum of flexural modes in graphene are responsible for almost

fourfold higher interfacial conductances with a much more pronounced temperature dependence as compared to MoS_2-based heterostructures. However, we also show that increasing the anharmonic interactions within the MoS_2 layer by increasing the van der Waals interaction strength with the 3D substrate can drastically enhance the interfacial conductances. Our results provide the fundamental understanding of the microscopic physical processes dictating interfacial heat flow across 2D-material interfaces, and as such, will be critical for the further development of the next generation of technologies utilizing 2D-3D heterostructures through their proper thermal management strategies.

ACKNOWLEDGMENTS

This work is supported by the Office of Naval Research, Grant No. N00014-21-1-2622. The work is also partially supported by the National Science Foundation (NSF Award No. 2119365).

[1] N. Li, Q. Wang, C. Shen, Z. Wei, H. Yu, J. Zhao, X. Lu, G. Wang, C. He, and L. Xie, *et al.*, Large-scale flexible and transparent electronics based on monolayer molybdenum disulfide field-effect transistors, Nat. Electron. **3**, 711 (2020).

[2] R. Cheng, J. Bai, L. Liao, H. Zhou, Y. Chen, L. Liu, Y.-C. Lin, S. Jiang, Y. Huang, and X. Duan, High-frequency self-aligned graphene transistors with transferred gate stacks, Proc. Natl. Acad. Sci. **109**, 11588 (2012).

[3] L. Britnell, R. Gorbachev, R. Jalil, B. Belle, F. Schedin, A. Mishchenko, T. Georgiou, M. Katsnelson, L. Eaves, and S. Morozov, *et al.*, Field-effect tunneling transistor based on vertical graphene heterostructures, Science **335**, 947 (2012).

[4] R. J. Warzoha, A. A. Wilson, B. F. Donovan, N. Donmezer, A. Giri, P. E. Hopkins, S. Choi, D. Pahinkar, J. Shi, and S. Graham, *et al.*, Applications and impacts of nanoscale thermal transport in electronics packaging, J. Electron. Packag. **143**, 020804 (2021).

[5] T. Roy, M. Tosun, J. S. Kang, A. B. Sachid, S. B. Desai, M. Hettick, C. C. Hu, and A. Javey, Field-effect transistors built from all two-dimensional material components, ACS Nano **8**, 6259 (2014).

[6] A. Giri and P. E. Hopkins, A review of experimental and computational advances in thermal boundary conductance and nanoscale thermal transport across solid interfaces, Adv. Funct. Mater. **30**, 1903857 (2020).

[7] E. Yalon, B. Aslan, K. K. Smithe, C. J. McClellan, S. V. Suryavanshi, F. Xiong, A. Sood, C. M. Neumann, X. Xu, and K. E. Goodson, *et al.*, Temperature-dependent thermal boundary conductance of monolayer MoS_2 by Raman thermometry, ACS Appl. Mater. Interfaces **9**, 43013 (2017).

[8] C. J. Foss and Z. Aksamija, Quantifying thermal boundary conductance of 2D–3D interfaces, 2D Mater. **6**, 025019 (2019).

[9] Q. H. Wang, K. Kalantar-Zadeh, A. Kis, J. N. Coleman, and M. S. Strano, Electronics and optoelectronics of two-dimensional transition metal dichalcogenides, Nat. Nanotechnol. **7**, 699 (2012).

[10] F. Xia, H. Wang, D. Xiao, M. Dubey, and A. Ramasubramaniam, Two-dimensional material nanophotonics, Nat. Photon. **8**, 899 (2014).

[11] C. Liu, H. Chen, S. Wang, Q. Liu, Y.-G. Jiang, D. W. Zhang, M. Liu, and P. Zhou, Two-dimensional materials for next-generation computing technologies, Nat. Nanotechnol. **15**, 545 (2020).

[12] P. Hopkins, ISRN mechanical engineering, **682586**, 2013.

[13] E. Yalon, C. J. McClellan, K. K. Smithe, M. Muñoz Rojo, R. L. Xu, S. V. Suryavanshi, A. J. Gabourie, C. M. Neumann, F. Xiong, and A. B. Farimani, *et al.*, Energy dissipation in monolayer MoS_2 electronics, Nano Lett. **17**, 3429 (2017).

[14] A. Behranginia, Z. Hemmat, A. K. Majee, C. J. Foss, P. Yasaei, Z. Aksamija, and A. Salehi-Khojin, Power dissipation of WSe_2 field-effect transistors probed by low-frequency Raman thermometry, ACS Appl. Mater. Interfaces **10**, 24892 (2018).

[15] B. M. Foley, S. C. Hernandez, J. C. Duda, J. T. Robinson, S. G. Walton, and P. E. Hopkins, Modifying surface energy of graphene via plasma-based chemical functionalization to tune thermal and electrical transport at metal interfaces, Nano Lett. **15**, 4876 (2015).

[16] P. E. Hopkins, M. Baraket, E. V. Barnat, T. E. Beechem, S. P. Kearney, J. C. Duda, J. T. Robinson, and S. G. Walton, Manipulating thermal conductance at metal–graphene contacts via chemical functionalization, Nano Lett. **12**, 590 (2012).

[17] Y. K. Koh, M.-H. Bae, D. G. Cahill, and E. Pop, Heat conduction across monolayer and few-layer graphenes, Nano Lett. **10**, 4363 (2010).

[18] Z. Chen, W. Jang, W. Bao, C. Lau, and C. Dames, Thermal contact resistance between graphene and silicon dioxide, Appl. Phys. Lett. **95**, 161910 (2009).

[19] X. Li, Y. Yan, L. Dong, J. Guo, A. Aiyiti, X. Xu, and B. Li, Thermal conduction across a boron nitride and SiO_2 interface, J. Phys. D: Appl. Phys. **50**, 104002 (2017).

[20] P. Yasaei, C. J. Foss, K. Karis, A. Behranginia, A. I. El-Ghandour, A. Fathizadeh, J. Olivares, A. K. Majee, C. D. Foster, and F. Khalili-Araghi, *et al.*, Interfacial thermal transport in monolayer MoS_2-and graphene-based devices, Adv. Mater. Interfaces **4**, 1700334 (2017).

[21] P. Yasaei, Z. Hemmat, C. J. Foss, S. J. Li, L. Hong, A. Behranginia, L. Majidi, R. F. Klie, M. W. Barsoum, and Z. Aksamija, *et al.*, Enhanced thermal boundary conductance in few-layer Ti_3C_2 MXene with encapsulation, Adv. Mater. **30**, 1801629 (2018).

[22] J. Yang, E. Ziade, C. Maragliano, R. Crowder, X. Wang, M. Stefancich, M. Chiesa, A. K. Swan, and A. J. Schmidt, Thermal conductance imaging of graphene contacts, J. Appl. Phys. **116**, 023515 (2014).

[23] P. Yasaei, A. Behranginia, Z. Hemmat, A. I. El-Ghandour, C. D. Foster, and A. Salehi-Khojin, Quantifying the limits of through-plane thermal dissipation in 2D-material-based systems, 2D Mater. **4**, 035027 (2017).

[24] Z.-Y. Ong, B. Qiu, S. Xu, X. Ruan, and E. Pop, Flexural resonance mechanism of thermal transport across graphene-SiO_2 interfaces, J. Appl. Phys. **123**, 115107 (2018).
[25] T. Feng, W. Yao, Z. Wang, J. Shi, C. Li, B. Cao, and X. Ruan, Spectral analysis of nonequilibrium molecular dynamics: Spectral phonon temperature and local nonequilibrium in thin films and across interfaces, Phys. Rev. B **95**, 195202 (2017).
[26] Z. Xu and M. J. Buehler, Heat dissipation at a graphene–substrate interface, J. Phys.: Condens. Matter **24**, 475305 (2012).
[27] H. Wang, J. Gong, Y. Pei, and Z. Xu, Thermal transfer in graphene-interfaced materials: Contact resistance and interface engineering, ACS Appl. Mater. Interfaces **5**, 2599 (2013).
[28] J. Zhang, Y. Hong, Z. Tong, Z. Xiao, H. Bao, and Y. Yue, Molecular dynamics study of interfacial thermal transport between silicene and substrates, Phys. Chem. Chem. Phys. **17**, 23704 (2015).
[29] H. Zhang, H. Wang, S. Xiong, H. Han, S. Volz, and Y. Ni, Multiscale modeling of heat dissipation in 2D transistors based on phosphorene and silicene, J. Phys. Chem. C **122**, 2641 (2018).
[30] S. V. Suryavanshi, A. J. Gabourie, A. Barati Farimani, and E. Pop, Thermal boundary conductance of two-dimensional MoS_2 interfaces, J. Appl. Phys. **126**, 055107 (2019).
[31] G. C. Correa, C. J. Foss, and Z. Aksamija, Interface thermal conductance of van der Waals monolayers on amorphous substrates, Nanotechnology **28**, 135402 (2017).
[32] B. Persson, A. Volokitin, and H. Ueba, Phononic heat transfer across an interface: Thermal boundary resistance, J. Phys.: Condens. Matter **23**, 045009 (2011).
[33] B. Persson and H. Ueba, Heat transfer between graphene and amorphous SiO_2, J. Phys.: Condens. Matter **22**, 462201 (2010).
[34] Z.-Y. Ong, Y. Cai, and G. Zhang, Theory of substrate-directed heat dissipation for single-layer graphene and other two-dimensional crystals, Phys. Rev. B **94**, 165427 (2016).
[35] J. C. Duda, J. L. Smoyer, P. M. Norris, and P. E. Hopkins, Extension of the diffuse mismatch model for thermal boundary conductance between isotropic and anisotropic materials, Appl. Phys. Lett. **95**, 031912 (2009).
[36] J. C. Duda, P. E. Hopkins, T. E. Beechem, J. L. Smoyer, and P. M. Norris, Inelastic phonon interactions at solid–graphite interfaces, Superlattices Microstruct. **47**, 550 (2010).
[37] S. Plimpton, Fast parallel algorithms for short-range molecular dynamics, J. Comput. Phys. **117**, 1 (1995).
[38] A. Kandemir, H. Yapicioglu, A. Kinaci, T. Çağın, and C. Sevik, Thermal transport properties of MoS_2 and $MoSe_2$ monolayers, Nanotechnology **27**, 055703 (2016).
[39] S. J. Stuart, A. B. Tutein, and J. A. Harrison, A reactive potential for hydrocarbons with intermolecular interactions, J. Chem. Phys. **112**, 6472 (2000).
[40] A. Giri and P. E. Hopkins, Resonant phonon modes in fullerene functionalized graphene lead to large tunability of thermal conductivity without impacting the mechanical properties, J. Appl. Phys. **125**, 205102 (2019).
[41] M. Noshin, A. I. Khan, I. A. Navid, H. A. Uddin, and S. Subrina, Impact of vacancies on the thermal conductivity of graphene nanoribbons: A molecular dynamics simulation study, AIP Adv. **7**, 015112 (2017).
[42] C. Si, X.-D. Wang, Z. Fan, Z.-H. Feng, and B.-Y. Cao, Impacts of potential models on calculating the thermal conductivity of graphene using non-equilibrium molecular dynamics simulations, Int. J. Heat Mass Transf. **107**, 450 (2017).
[43] S. Munetoh, T. Motooka, K. Moriguchi, and A. Shintani, Interatomic potential for Si–O systems using Tersoff parameterization, Comput. Mater. Sci. **39**, 334 (2007).
[44] P. K. Schelling, S. R. Phillpot, and P. Keblinski, Comparison of atomic-level simulation methods for computing thermal conductivity, Phys. Rev. B **65**, 144306 (2002).
[45] J. M. Larkin and A. J. McGaughey, Thermal conductivity accumulation in amorphous silica and amorphous silicon, Phys. Rev. B **89**, 144303 (2014).
[46] C. Abs da Cruz, K. Termentzidis, P. Chantrenne, and X. Kleber, Molecular dynamics simulations for the prediction of thermal conductivity of bulk silicon and silicon nanowires: Influence of interatomic potentials and boundary conditions, J. Appl. Phys. **110**, 034309 (2011).
[47] R. Xiang, T. Inoue, Y. Zheng, A. Kumamoto, Y. Qian, Y. Sato, M. Liu, D. Tang, D. Gokhale, and J. Guo, *et al.*, One-dimensional van der Waals heterostructures, Science **367**, 537 (2020).
[48] J.-W. Jiang, H. S. Park, and T. Rabczuk, Molecular dynamics simulations of single-layer molybdenum disulphide (MoS_2): Stillinger-Weber parametrization, mechanical properties, and thermal conductivity, J. Appl. Phys. **114**, 064307 (2013).
[49] A. K. Rappé, C. J. Casewit, K. Colwell, W. A. Goddard III, and W. M. Skiff, UFF, a full periodic table force field for molecular mechanics and molecular dynamics simulations, J. Am. Chem. Soc. **114**, 10024 (1992).
[50] See Supplemental Material at http://link.aps.org/supplemental/10.1103/PhysRevApplied.20.014039 for universal force-field parameters for Lennard-Jones (LJ) potential used to model our 2D-3D interfaces; further details of nonequilibrium molecular dynamics simulations and vibrational density of states; schematic illustrations of the computational domains for our 2D-3D heterostructures; spectral energy density for crystalline silicon.
[51] W. G. Hoover, Canonical dynamics: Equilibrium phase-space distributions, Phys. Rev. A **31**, 1695 (1985).
[52] S. Thakur, C. J. Dionne, P. Karna, S. W. King, W. Lanford, H. Li, S. Banerjee, D. Merrill, P. E. Hopkins, and A. Giri, Density and atomic coordination dictate vibrational characteristics and thermal conductivity of amorphous silicon carbide, Phys. Rev. Mater. **6**, 094601 (2022).
[53] A. Giri, C. J. Dionne, and P. E. Hopkins, Atomic coordination dictates vibrational characteristics and thermal conductivity in amorphous carbon, npj Comput. Mater. **8**, 55 (2022).
[54] A. Giri, P. E. Hopkins, J. G. Wessel, and J. C. Duda, Kapitza resistance and the thermal conductivity of amorphous superlattices, J. Appl. Phys. **118**, 165303 (2015).
[55] J. A. Thomas, J. E. Turney, R. M. Iutzi, C. H. Amon, and A. J. McGaughey, Predicting phonon dispersion relations and lifetimes from the spectral energy density, Phys. Rev. B **81**, 081411 (2010).

[56] J. A. Thomas, J. E. Turney, R. M. Iutzi, C. H. Amon, and A. J. McGaughey, Erratum: Predicting phonon dispersion relations and lifetimes from the spectral energy density [Phys. Rev. B 81, 081411 (r)(2010)], Phys. Rev. B **91**, 239905 (2015).

[57] K. Sääskilahti, J. Oksanen, J. Tulkki, and S. Volz, Role of anharmonic phonon scattering in the spectrally decomposed thermal conductance at planar interfaces, Phys. Rev. B **90**, 134312 (2014).

[58] A. Giri, J. L. Braun, and P. E. Hopkins, Implications of interfacial bond strength on the spectral contributions to thermal boundary conductance across solid, liquid, and gas interfaces: A molecular dynamics study, J. Phys. Chem. C **120**, 24847 (2016).

[59] A. J. Gabourie, Ç. Köroğlu, and E. Pop, Substrate-dependence of monolayer MoS_2 thermal conductivity and thermal boundary conductance, J. Appl. Phys. **131**, 195103 (2022).

[60] E. Landry and A. McGaughey, Thermal boundary resistance predictions from molecular dynamics simulations and theoretical calculations, Phys. Rev. B **80**, 165304 (2009).

[61] P. E. Hopkins, J. A. Tomko, and A. Giri, Quasi-harmonic theory for phonon thermal boundary conductance at high temperatures, J. Appl. Phys. **131**, 015101 (2022).

[62] S. Sadasivam, Y. Che, Z. Huang, L. Chen, S. Kumar, and T. S. Fisher, The atomistic Green's function method for interfacial phonon transport, Annu. Rev. Heat Transfer **17**, 89 (2014).

[63] N. Mingo and L. Yang, Phonon transport in nanowires coated with an amorphous material: An atomistic Green's function approach, Phys. Rev. B **68**, 245406 (2003).

[64] M. Li, J. Zhang, X. Hu, and Y. Yue, Thermal transport across graphene/SiC interface: Effects of atomic bond and crystallinity of substrate, Appl. Phys. A **119**, 415 (2015).

[65] Q. Wang, J. Zhang, Y. Xiong, S. Li, V. Chernysh, and X. Liu, Atomic-scale surface engineering for giant thermal transport enhancement across 2D/3D van der Waals interfaces, ACS Appl. Mater. & Interfaces (2023).

[66] A. Ipatov, D. Parshin, and D. Conyuh, Dispersion of flexural modes in graphene, J. Exp. Theor. Phys. **133**, 461 (2021).

[67] C. Foss and Z. Aksamija, Thermal boundary conductance of monolayer beyond-graphene two-dimensional materials on SiO_2 and GaN, Nanotechnology **32**, 405206 (2021).

[68] Z.-Y. Ong and E. Pop, Effect of substrate modes on thermal transport in supported graphene, Phys. Rev. B **84**, 075471 (2011).

[69] X. Li, L. Tao, Z. Chen, H. Fang, X. Li, X. Wang, J.-B. Xu, and H. Zhu, Graphene and related two-dimensional materials: Structure-property relationships for electronics and optoelectronics, Appl. Phys. Rev. **4**, 021306 (2017).

[70] A. Daus, S. Vaziri, V. Chen, Ç. Köroğlu, R. W. Grady, C. S. Bailey, H. R. Lee, K. Schauble, K. Brenner, and E. Pop, High-performance flexible nanoscale transistors based on transition metal dichalcogenides, Nat. Electron. **4**, 495 (2021).